Wang et al. *Zool. Res.* 2026, 47(2): 429−443
https://doi.org/10.24272/j.issn.2095-8137.2025.181
https://cstr.cn/32248.14.zr.2025.181

ZR | Zoological Research

Article Open Access

Deficiency of *pnkp* in zebrafish causes microcephaly, seizures, and developmental delay through mitochondrial dysfunction

Gui-Hua Wang[1], Ling-Lu Xiao[1], Wei-Min Jia[1], Zhen-Xing Liu[1], Hai-Bo Jia[1], Yan-Xi Sun[2], Zhi-Ke Zi[2,*], Xian-Qin Zhang[1,*]

[1] *Key Laboratory of Molecular Biophysics of the Ministry of Education*, *College of Life Science and Technology and Center for Human Genome Research*, *Huazhong University of Science and Technology*, *Wuhan*, *Hubei* 430074, *China*

[2] *State Key Laboratory of Quantitative Synthetic Biology*, *Shenzhen Institute of Synthetic Biology*, *Shenzhen Institutes of Advanced Technology*, *Chinese Academy of Sciences*, *Shenzhen*, *Guangdong* 518055, *China*

ABSTRACT

Variants in *PNKP* cause a severe neurodevelopmental disorder characterized by microcephaly, seizures, and developmental delay (MCSZ). Despite clear clinical significance, the pathological mechanisms underlying this condition remain incompletely understood. In this study, CRISPR/Cas9 genome editing was applied to generate a zebrafish *pnkp* knockout model (*pnkp*$^{-/-}$), overcoming limitations associated with previously reported mouse models that exhibited postnatal lethality. The *pnkp*$^{-/-}$ zebrafish faithfully recapitulated key phenotypic traits observed in human *PNKP* deficiency, facilitating in-depth exploration of the molecular mechanisms contributing to disease. Loss of *PNKP* function resulted in mitochondrial DNA damage, accompanied by disruption of mitochondrial ultrastructure and bioenergetic function, increased apoptosis, and reduced autophagic activity, collectively leading to pronounced cerebral neurodevelopmental abnormalities. Transcriptomic analysis based on RNA sequencing identified marked down-regulation of gamma-aminobutyric acid (GABA) receptor-related genes. Pharmacological activation of $GABA_A$ receptors with muscimol partially rescued hyperactive behavior in *pnkp*$^{-/-}$ zebrafish, suggesting a potential link between GABAergic signaling and seizure-related phenotypes. Drug screening performed using the *pnkp*$^{-/-}$ zebrafish model further identified lamotrigine as a comparatively effective compound for seizure control associated with *PNKP* mutations. These findings clarify mechanistic links between *PNKP* deficiency and MCSZ pathology, identify candidate therapeutic agents, and provide an experimental framework for investigation of disorders associated with defective DNA repair.

Keywords: *PNKP*; Autophagy; Apoptosis; Zebrafish; Drug screening

INTRODUCTION

Variants in the human *PNKP* gene cause an autosomal recessive neurological abnormality characterized primarily by microcephaly, seizures, and developmental delay (MCSZ) (Shen et al., 2010). PNKP functions as a DNA end-processing enzyme that restores DNA termini prior to ligation during DNA repair (Reynolds et al., 2012). This protein represents a bifunctional DNA repair factor with both 5'-kinase and 3'-phosphatase activities and contains three principal structural domains: a C-terminal catalytic kinase region, a phosphatase domain, and an N-terminal forkhead-associated (FHA) domain (Bernstein et al., 2005). The FHA domain mediates interactions with X-ray repair cross complementing protein 1 (XRCC1) during base excision repair (BER) and recognizes XRCC4 during non-homologous end joining (NHEJ) (Koch et al., 2004; Shin et al., 2021). Subcellular localization of PNKP occurs in both the nucleus and mitochondria, playing a critical role in the repair of mitochondrial DNA (mtDNA) damage (Tahbaz et al., 2012). Deficiency of *Pnkp* results in severe mtDNA abnormalities that contribute to diverse human pathologies, including cancer, age-associated disorders, and mitochondrial diseases (Damas et al., 2014; Fontana & Gahlon, 2020). Mitochondria regulate multiple cellular processes, including apoptosis, oxidative stress responses, and mitophagy (Akbari et al., 2022; Gahl et al., 2016). Dysfunction of mitochondrial homeostasis has been implicated in various diseases and is particularly detrimental to the

Received: 10 July 2025; Accepted: 15 September 2025; Online: 16 September 2025

Foundation items: This work was supported by the National Key R&D Program of China (2023YFC2706302), National Natural Science Foundation of China (81000079, 81170165 and 81870959 to X.Q.Z., 32471293 to Z.K.Z.), Program of HUST Academic Frontier Youth Team (2016QYTD02), Fundamental Research Funds for the Central Universities (HUST: 2019JYCXJJ035)

*Corresponding authors, E-mail: zk.zi@siat.ac.cn; xqzhang04@hust.edu.cn

nervous system due to the high energetic requirements of neural tissue (Zheng et al., 2019). Although involvement of *PNKP* in mtDNA repair is well-established in human cells, the specific mechanisms by which PNKP deficiency disrupts mitochondrial function and contributes to encephalopathy and seizure remain incompletely defined.

Autophagy represents a conserved cellular pathway responsible for degradation of excess proteins and clearance of damaged organelles in eukaryotic cells. DNA and mtDNA damage can trigger autophagy and mitophagy, respectively (Chen et al., 2020; Dan et al., 2020). Mitophagy constitutes a specialized autophagic process that selectively removes dysfunctional mitochondria to preserve mitochondrial quality and cellular homeostasis (Baechler et al., 2019). Regulatory pathways governing mitophagy include ubiquitin-dependent mechanisms mediated by PTEN-induced kinase 1 (PINK1) and Parkin, as well as ubiquitin-independent pathways regulated by receptor proteins (Choi et al., 2021). Extensive investigation of the PINK1-Parkin pathway has demonstrated that impaired mitochondrial membrane potential (MMP) prevents PINK1 import across the mitochondrial inner membrane, leading to accumulation on the outer membrane and subsequent activation of Parkin, which promotes ubiquitination of mitochondrial proteins and initiates mitophagic clearance (Riley et al., 2013). Although dysregulation of autophagy has been associated with multiple neurological disorders (Wu et al., 2018), the molecular mechanisms linking *PNKP* deficiency to autophagy regulation and seizure development remain largely unexplored.

Homozygous *Pnkp* mutant mice exhibit postnatal lethality, limiting investigation of disease mechanisms in mammalian models (Shimada et al., 2015). Because MCSZ arises from biallelic pathogenic variants in *PNKP*, establishment of a viable homozygous mutant model represents a crucial step toward elucidation of disease pathogenesis. In the present study, CRISPR/Cas9 genome editing was used to generate a stable homozygous *pnkp* knockout zebrafish (*Danio rerio*) model. Zebrafish larvae carrying homozygous *pnkp* disruption exhibited phenotypic characteristics consistent with MCSZ observed in patients harboring *PNKP* variants. Analysis of *pnkp*-deficient zebrafish revealed profound effects on early brain development and behavioral activity. The cellular mechanisms underlying these phenotypes were further examined through gene knockdown experiments in HEK293T cells to assess functional consequences of *PNKP* deficiency. Collectively, the results of this study provide a framework for elucidating the molecular mechanisms by which *PNKP* deficiency disrupts mitochondrial homeostasis and contributes to neurodevelopmental abnormalities associated with MCSZ.

MATERIALS AND METHODS

Zebrafish maintenance and generation of *pnkp*-mutant zebrafish

All zebrafish were maintained at 28.5°C under a 14 h light/10 h dark cycle with lights on from 0800h to 2200h. Embryos were obtained from the AB wild-type (WT) strain. All husbandry procedures and experimental protocols were conducted in accordance with the guidelines of the Ethics Committee of the College of Life Science and Technology, Huazhong University of Science and Technology ([2021] IACUC Number: 3083). A *pnkp* knockout zebrafish line was established using CRISPR/Cas9-mediated genome editing. Single guide RNAs (sgRNAs) targeting the *pnkp* locus were designed using the CHOPCHOP platform (http://chopchop.cbu.uib.no/). The sgRNAs were transcribed *in vitro* using TranscriptAid T7 High Yield Transcription Kit (Thermo Scientific, USA). Approximately 100 pg of sgRNA together with 500 pg of recombinant Cas9 protein (ST-SC-004, Eastinno Biotechnology Co. Ltd., China) was microinjected into embryos at the one- to two-cell stage. Genotyping was performed using two pairs of primers (Supplementary Table S1).

Morphological analysis

Zebrafish larvae at 3 and 5 days post-fertilization (dpf) were anesthetized with MS-222 and gently positioned on glass slides containing 1% methylcellulose for imaging. Dorsal and lateral views were acquired using an optical microscope. Morphometric parameters, including body length, eye area, and head surface area, were measured using ImageJ software.

Behavioral analysis

Larval behavioral activity was assessed using the DanioVision tracking system (Noldus, Netherlands). At 5 dpf, larvae were individually transferred to 96-well plates on the evening preceding experimentation to allow acclimation prior to spontaneous locomotor analysis. Activity was recorded during both light and dark conditions for 10 min per period. Responses were subsequently evaluated under alternating light-dark cycles consisting of 5 min of illumination followed by 5 min of darkness, repeated three times. Startle responses were induced using a dark-flash paradigm comprising 200 stimulus pulses of 0.5 s duration separated by 2 s intervals of darkness.

Pentylenetetrazole (PTZ) and muscimol were purchased from Macklin Inc. (China). Ethosuximide (ETX), carbamazepine (CBZ), lamotrigine (LTG), and rapamycin were purchased from Aladdin (China). Compounds were dissolved in embryonic medium or dimethyl sulfoxide (DMSO) to prepare stock solutions, which were then directly added to 96-well plates to achieve the required final concentrations. For pharmacological assays, ETX (25 μmol/L), CBZ (200 μmol/L), LTG (100 μmol/L), rapamycin (0.3 μmol/L), and muscimol (100 μmol/L) were administered to 5 dpf larvae 20 min or 20 h prior to behavioral recording. Extended rapamycin exposure was performed using 0.1 μmol/L from 0 hours post-fertilization (hpf) to 2 dpf and 0.3 μmol/L from 2 dpf to 5 dpf. PTZ treatment was performed using a concentration gradient of 1.25, 2.5, 5, 10, and 20 mmol/L for 20 min before tracking. Locomotor parameters, including total distance traveled and swimming velocity, were quantified by EthoVision XT 14 (Noldus, Netherlands). Movement was classified into three velocity categories according to established criteria (Winter et al., 2008): low velocity (<5 mm/s), medium velocity (5–20 mm/s), and high velocity (>20 mm/s). High-velocity activity was interpreted as hyperactive locomotor behavior.

Quantitative and semi-quantitative reverse transcription-polymerase chain reaction (RT-qPCR and semi-RT-PCR)

Total RNA was extracted from the heads of zebrafish larvae at 3 dpf and 5 dpf (15–20 individuals per sample) using TRIzol reagent (Invitrogen, USA). RNA quantity and quality were evaluated using a NanoDrop 2000 spectrophotometer (Thermo, USA) and agarose gel electrophoresis, respectively. For cDNA synthesis, 100 ng of total RNA was reverse-

transcribed using HiScript II Q RT SuperMix for qPCR (+gDNA wiper) (R223- 01, Vazyme, China) according to the manufacturer's instructions. RT-qPCR was performed using Hieff qPCR SYBR Green Master Mix (HB210910, Yeasen, China) on a StepOnePlus Real-Time PCR system (Life Technologies, USA). Relative transcript abundance was calculated using the $2^{-\Delta\Delta Ct}$ method with *β-actin* normalization. Semi-RT-PCR products were resolved by electrophoresis on 2% agarose gels and visualized using a gel documentation system (Bio-Rad, USA). Band intensity was analyzed using ImageJ software. Primer sequences are listed in Supplementary Table S1.

Long-range quantitative PCR (LR-PCR)

Zebrafish mtDNA damage was assessed using LR-PCR to amplify extended mtDNA fragments according to previously described methods (Liu et al., 2008, 2015). Genomic DNA was isolated using the Qiagen Genomic DNA Isolation Kit (4991107, Qiagen, China), following the manufacturer's instructions. The mitochondrial genome was amplified as two overlapping fragments of approximately 8 kb and 8.4 kb. Amplification of mitochondrial NADH dehydrogenase subunit 1 (mt*ND1*) by semi-quantitative PCR served as a normalization control for DNA input. LR-PCR analysis was conducted using LA Taq® (RR02MA, TaKaRa, Japan). Amplified products were subjected to electrophoresis on a 0.8% agarose gel. Relative mtDNA abundance was quantified using ImageJ. All primer sequences are provided in Supplementary Table S1.

Western blot analysis

Total protein extracts were prepared from heads of zebrafish larvae at 3 dpf or 5 dpf (20–30 individuals per sample) or from HEK293T cells using RIPA buffer (Beyotime, China) supplemented with complete protease inhibitor (Roche, Switzerland). Samples were homogenized using a tissue grinder followed by six cycles of vortex disruption within 30 min. Homogenates were subsequently subjected to sonication using an ultrasonic cell disruptor. After centrifugation at 12 000 r/min for 20 min at 4 °C, supernatants containing total proteins were collected and denatured in sodium dodecyl sulfate (SDS) loading buffer by incubation at 95°C for 10 min.

Denatured protein samples were separated by sodium dodecyl sulfate-polyacrylamide gel electrophoresis (SDS-PAGE) at 80 V and transferred to polyvinylidene fluoride (PVDF) membranes. The membranes were blocked for 2 h with western blot blocking solution consisting of 5% skimmed milk in TBST and subsequently incubated overnight at 4°C with primary antibodies. The membranes were then incubated with horseradish peroxidase (HRP)-conjugated secondary antibodies for 2 h. Immunoreactive signals were detected using chemiluminescence with the ChemiDoc XRS+ imaging system (Bio-Rad, USA). Antibodies used in this study included: anti-GAPDH (GB12001, Servicebio, China; 1:1 000), anti-actin (GB12002, Servicebio, China, 1:1 000), anti-PNKP (A6693, ABclonal, China, 1:1 000), anti-p53 (GTX128135, Genetex, China, 1:1 000), anti-γH2AX (Cat#2577, CST, USA, 1:1 000), anti-BAX (T40051F, Abmart, China, 1:2 000), anti-BCL-2 (T40056F, Abmart, China, 1:2 000), anti-APAF-1 (380882, ZenBio, China, 1:1 000), anti-BCL-XL (T40057F, Abmart, China, 1:1 000), anti-p-ATM (Cat#380751, CST, USA, 1:1 000), anti-p-ATR (AP0676, ABclon, China, 1:500), anti-p-CHK1 (310037, ZenBio, China, 1:1 000), anti-p-CHK2 (TP56120F, Abmart, China, 1:1 000), anti-DRP1 (Cat#340336, CST, USA, 1:1 000), anti-FIS1 (R26001, ZenBio, China, 1:1 000), anti-DYN2 (Cat#861637, CST, USA, 1:1 000), anti-OPA1 (R382025, ZenBio, China, 1:1 000), anti-SOD2 (Cat#306028, CST, USA, 1:1 000), anti-LC3 (14600-1-AP, Proteintech, USA, 1:1 000), anti-p62 (T55546F, Abmart, China, 1:1 000), anti-ATG5 (T55766, Abmart, China, 1:2 000), anti-Beclin1 (A11761, ABclon, China, 1:1 000), anti-Parkin (R381626, ZenBio, China, 1:1 000), anti-PINK1 (23274-1-AP, Proteintech, USA, 1:500), anti-Mitofilin (NCTP05421, Saierbio, China, 1:1 000), anti-COXIV (200147, ZenBio, China, 1:1 000), anti-mTOR (T55306, Abmart, China, 1:1 000), anti-p-mTOR (T56571F, Abmart, China, 1:1 000), anti-S6 (R25622, ZenBio, China, 1:1 000), anti-p-S6 (R25622, ZenBio, China, 1:1 000).

Cell apoptosis detection

Zebrafish larvae at 5 dpf were collected alive and fixed in 4% paraformaldehyde (PFA) for 4–6 h at room temperature. Samples were washed twice with phosphate-buffered saline (PBS) for 5 min per wash and subsequently dehydrated in methanol for 30 min at −20°C Larvae were rinsed three times with PBS containing Tween-20 (PBST) for 5 min each and digested with 20 μg/mL proteinase K for 1 h at room temperature. Samples were equilibrated in equilibration buffer for 30 min and incubated with terminal deoxynucleotidyl transferase-mediated dUTP nick-end labeling (TUNEL) reaction mixture overnight in darkness at 4°C, using the TUNEL Bright Green Apoptosis Detection Kit (A112-03, Vazyme, China) according to the manufacturer's protocols. The following day, TUNEL-labeled larvae were incubated at 37°C for 1 h and washed with PBST. Nuclear staining was performed using Hoechst 33342 (Beyotime Biotechnology, China) for 5 min in darkness, followed by PBST washing. TUNEL-positive signals were observed using a confocal microscope (Olympus FV1000, Japan).

Cell culture and transfection

HEK293T cells were maintained in Dulbecco's Modified Eagle Medium (DMEM) (Gibco, USA) supplemented with 10% fetal bovine serum (FBS) (Invigentech, USA) in a 37°C incubator with 5% CO_2. For small interfering RNA (siRNA) transfection, cells were cultured in 6-well plates (Nest Biotechnology, China) with 1 mL of culture medium per well. A random negative control siRNA (siNC) lacking complementarity to any human gene served as control, whereas human PNKP-targeting siRNA (si*PNKP*; sequence 5-GGAAACGGGUCG CCAUCGA-3) was used for knockdown (Kalasova et al., 2020). Transfection was carried out using 5 nmol/L PNKP and control siRNA oligonucleotides with Lipofectamine 3000 transfection reagent (Invitrogen, USA) according to the manufacturer's protocols. After 72 h of incubation, cells were washed twice with PBS and collected for subsequent experiments.

Histological assay

Histological examination of zebrafish larvae was performed using paraffin sectioning followed by hematoxylin and eosin (H&E) staining. Larvae at 5 dpf were collected and fixed in 4% PFA overnight at 4°C. Samples were dehydrated through graded alcohol solutions, followed by infiltration with dimethylbenzene and sequential transfer into paraffin. Paraffin blocks were sectioned at 5 μm thickness and dried at 37°C. Slides were stained with H&E and imaged using a microscope.

Immunofluorescence assay

HEK293T cells were seeded onto 35 mm confocal dishes

(Biosharp, China). After transfection, cells were washed three times with PBS and fixed with 4% PFA for 15 min. Permeabilization was performed using 0.5% Triton X-100 (T8200, Solarbio, China) in PBS for 20 min, followed by blocking in 10% bovine serum albumin (BSA) in PBST for 30 min at room temperature. Cells were then incubated overnight at 4°C with primary antibodies including anti-cytochrome c (Cyt C; 1:500, T55734F, Abmart, China), anti-Mitofilin (1:500), anti-LC3 (1:500), and anti-COXIV (1:500). Cy3-conjugated goat anti-rabbit IgG (ABclon, China) and Alexa Fluor 488-conjugated goat anti-mouse IgG (Abcam, USA) were applied as secondary antibodies for 2 h at room temperature. Fluorescence images were acquired using a confocal microscope (Olympus, Japan).

Measurement of MMP and reactive oxygen species (ROS)

HEK293T cells were cultured in confocal dishes for fluorescence analysis. MMP was evaluated using 5,5′,6,6′-tetrachloro-1,1′,3,3′-tetraethyl-imidacarbocyanine (JC-1) staining (C2003S, Beyotime, China), and intracellular ROS levels were measured using the fluorescent probe 2',7'-dichlorodihydrofluorescein diacetate (DCFH-DA; S0033S, Beyotime, China). Staining procedures were conducted according to the manufacturer's instructions.

RNA-sequencing (RNA-seq) analysis

RNA-seq analysis was performed using three independent biological replicates for both WT and *pnkp*$^{-/-}$ zebrafish. For each replicate, 30 larvae at 5 dpf were dissected. Tail tissue was used for genotyping, and heads from homozygous mutants were selected for RNA extraction. Total RNA extracted from the heads of WT and *pnkp*$^{-/-}$ zebrafish was used for cDNA library construction. Sequencing libraries were prepared by Novogene (China) and analyzed using the Illumina sequencing platform. Sequence reads were aligned to the zebrafish reference genome (GRCz11) using HISAT2 v.2.0.4. Gene expression levels were quantified using HTSeq-count with intersection-strict mode. Differentially expressed genes (DEGs) were identified using DESeq2, applying cut-off thresholds of fold change (FC)≥2 and adjusted P≤0.05. Kyoto Encyclopedia of Genes and Genomes (KEGG) and Gene Ontology (GO) functional enrichment analyses were performed using DAVID (Huang et al., 2009).

Statistical analysis

All experiments were independently performed at least three times. Statistical analyses were conducted using GraphPad Prism v.6.0. Data are presented as mean±standard error of the mean (SEM). Significance testing between two groups was conducted using unpaired two-tailed Student *t*-tests, while differences among multiple groups were analyzed using one-way analysis of variance (ANOVA). Significance levels were defined as follows: *: P<0.05; **: P<0.01; ***: P<0.001; ****: P<0.0001; ns: Not significant.

RESULTS

***pnkp* knockout induces microcephaly, seizures, and developmental delay in zebrafish**

Expression dynamics of *pnkp* during early zebrafish development were first examined in WT embryos. Transcript abundance was quantified by RT-PCR across developmental stages. Persistent *pnkp* expression was observed from 0.2 hpf to 24 hpf, followed by a marked decline beginning at 36 hpf, indicating a prominent role during early embryogenesis (Supplementary Figure S1A). Tissue distribution analysis further demonstrated elevated *pnkp* expression in multiple organs, including the brain, heart, gallbladder, kidney, and testis, indicating its crucial functions in brain development (Supplementary Figure S1B).

Postnatal lethality in homozygous *Pnkp* mutant mice has limited investigation of the molecular mechanisms underlying MCSZ. To establish a viable vertebrate model, CRISPR/Cas9 genome editing was applied to disrupt the *pnkp* locus in zebrafish. Targeting exon 3 generated a two-base deletion (c.262–263delGT) that introduced a frameshift mutation and premature stop codon. This mutation triggered degradation of *pnkp* transcripts via nonsense-mediated mRNA decay (Figure 1A, B). Residual transcripts in *pnkp*$^{-/-}$ zebrafish larvae were predicted to encode a non-functional truncated protein terminating at p.V88*, resulting in the loss of approximately 500 amino acids and elimination of most functional domains required for Pnkp activity. Quantitative analysis confirmed markedly reduced mRNA expression levels in homozygous mutants at both 3 dpf and 5 dpf (Figure 1C), demonstrating successful generation of the *pnkp*$^{-/-}$ zebrafish model.

Developmental abnormalities were evident in *pnkp*$^{-/-}$ zebrafish embryos beginning at 1 hpf (Figure 1D). Mutant larvae exhibited significantly reduced body length at both 3 dpf and 5 dpf (Figure 1E), which persisted into adulthood (Supplementary Figure S1C). Pronounced reductions in head surface area, brain size, and cellular abundance were detected at 3 dpf and 5 dpf (Figure 1F, G). Quantitative assessment using the microcephaly index, defined as the ratio of eye distance to body length (Withers et al., 2023), revealed a significant decrease in *pnkp*$^{-/-}$ larvae at both developmental stages (Figure 1F). Consistent reductions in brain size were also observed in adult zebrafish (Supplementary Figure S1D). Collectively, these results demonstrate that *pnkp* deficiency produces microcephaly and developmental delay in zebrafish, closely recapitulating phenotypic characteristics associated with human *PNKP* variants.

Hyperactive behavior in *pnkp*$^{-/-}$ zebrafish

Given that loss-of-function *PNKP* variants are associated with seizure disorders in humans, *pnkp*$^{-/-}$ zebrafish behavior was evaluated by quantifying discrete locomotor parameters indicative of seizure- or anxiety-like activity (Kedra et al., 2020). Basal locomotor activity in 5 dpf *pnkp*$^{-/-}$ larvae was markedly elevated relative to WT larvae, characterized by increased total distance traveled and higher mean velocity of high-velocity movements (>20 mm/s) during both light and dark periods (Supplementary Figure S1E; Figure 2A, B). Notably, behavioral patterns differed between environmental conditions, with *pnkp*$^{-/-}$ larvae exhibiting pronounced hyperactivity under dark conditions and reduced movement under light conditions, suggesting that darkness exacerbated seizure- or anxiety-like behavioral responses.

Because transitions between light and darkness can markedly influence locomotor behavior (Baronio et al., 2022), activity was further examined across three consecutive light-dark cycles to provide a robust assessment of baseline locomotor dynamics. Persistent hyperactivity remained evident in *pnkp*$^{-/-}$ larvae, with the strongest behavioral responses occurring during dark intervals (Figure 2C, D). Sensitivity to environmental stimuli was subsequently examined through startle-response assays in 5 dpf larvae using repeated short

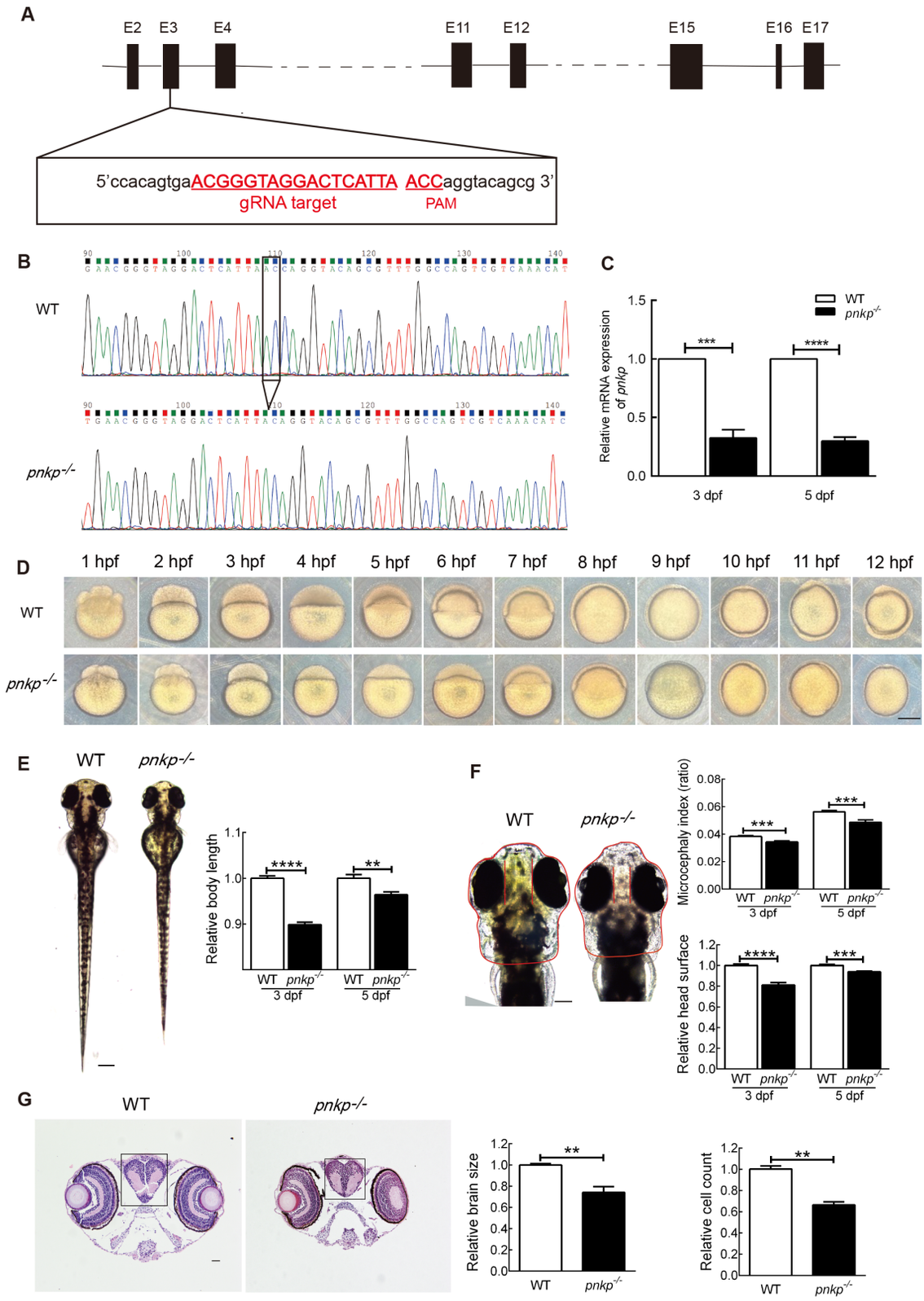

Figure 1 *pnkp* knockout induces MCSZ-associated phenotypes in zebrafish

A: Schematic illustration of CRISPR/Cas9 target site within *pnkp*. B: Sanger sequencing confirmed a 2 bp deletion in the *pnkp* genomic sequence. C: Relative *pnkp* mRNA expression in 3 dpf and 5 dpf larvae showing significant reduction in *pnkp*$^{-/-}$ individuals compared to WT controls (n=3). D: Developmental progression from 1 hpf to 12 hpf showing delayed development in *pnkp*$^{-/-}$ embryos beginning at 2 hpf relative to WT controls (n≥ 20 per genotype). Scale bar: 200 μm. E, F: Quantification of body length, head surface area, and microcephaly index (ratio of eye distance to body length) showing significant reduction in *pnkp*$^{-/-}$ larvae compared to WT controls at 3 dpf and 5 dpf (n≥20 per genotype). Scale bar: 200 μm or 80 μm. G: Brain size and cell count in 5 dpf larvae assessed by H&E staining showing reduced brain size and cellularity in *pnkp*$^{-/-}$ larvae compared with WT controls (n=3 per genotype). Black frame: larvae brain. Scale bar: 80 μm. Error bar denotes standard error of the mean (SEM). Significance was determined using unpaired two-tailed Student *t*-tests. ns: Not significant; **: P<0.01; ***: P<0.001; ****: P<0.0001.

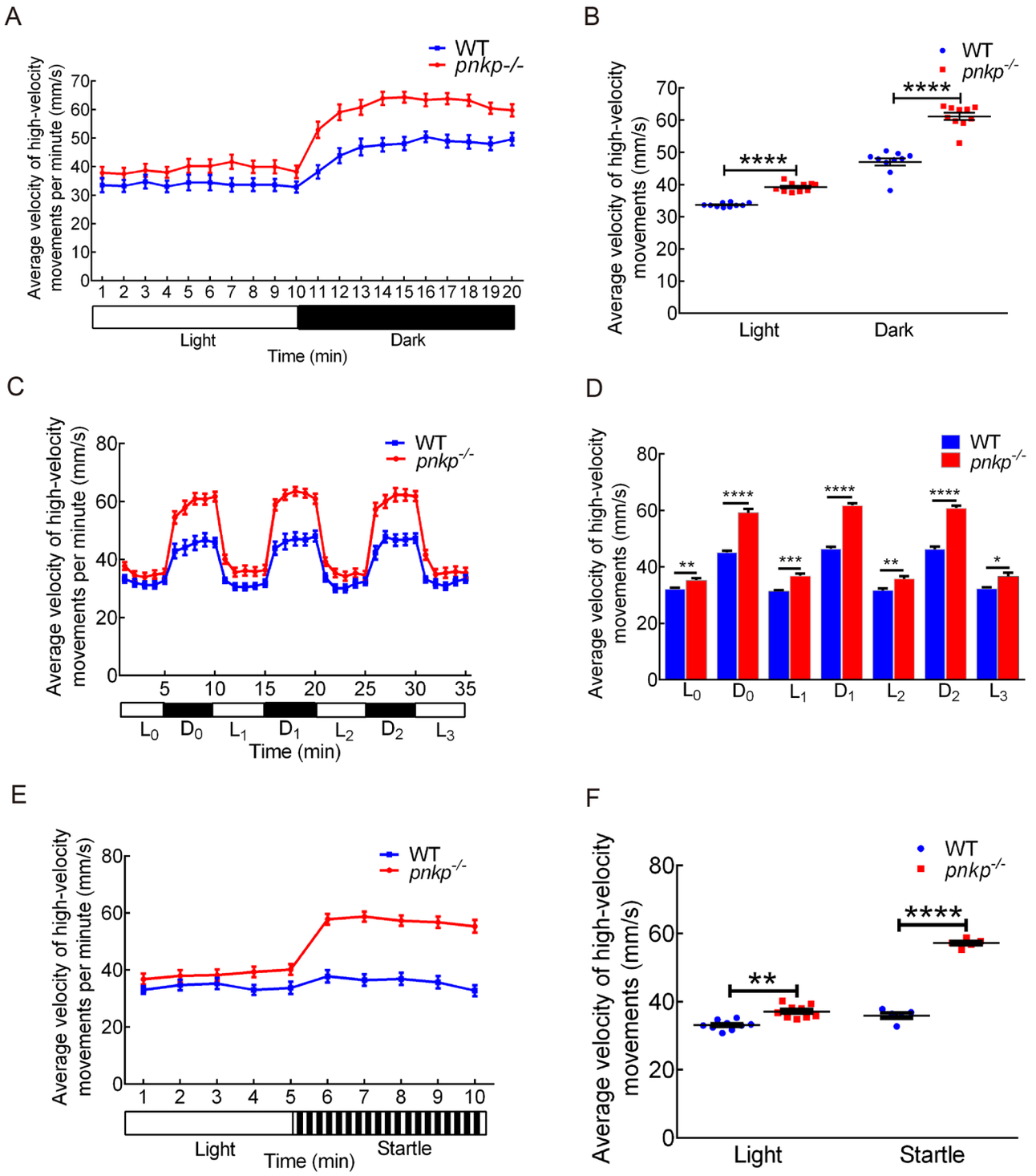

Figure 2 *pnkp* knockout induces hyperactive locomotor behavior in zebrafish larvae

High-velocity locomotor activity (>20 mm/s) was significantly increased in 5 dpf *pnkp*$^{-/-}$ larvae compared to WT controls under multiple illumination paradigms. A, B: Quantification of high-velocity movements under alternating light/dark conditions. C, D: Locomotor responses during repeated light-dark cycles. E, F: Locomotor responses under repeated short dark-flash stimulation (n≥20 per genotype). Error bar denotes standard error of the mean (SEM). Significance was determined using unpaired two-tailed Student t-tests. ns: Not significant; *: P<0.05; **: P<0.01; ***: P<0.001; ****: P<0.0001.

dark-flash stimuli. Under these conditions, *pnkp*$^{-/-}$ larvae displayed markedly enhanced hyperactive responses compared with WT larvae (Figure 2E, F), indicating that abrupt changes in illumination exacerbated seizure- or anxiety-like behavioral phenotypes.

Seizure susceptibility was further investigated using pharmacological challenge with PTZ, a γ-aminobutyric-acid receptor antagonist that induces epileptiform activity through noncompetitive antagonism of the $GABA_A$ receptor complex (Dhir, 2012). Unexpectedly, exposure of 5 dpf larvae to PTZ did not produce increased high-velocity locomotor bursts in *pnkp*$^{-/-}$ larvae compared with controls during the 20 min recording period (Supplementary Figure S1F). This lack of sensitivity to PTZ suggests potential dysfunction in GABAergic

neurons within *pnkp*$^{-/-}$ larvae.

Knockdown of *PNKP* leads to DNA damage

PNKP participates in two principal DNA damage repair pathways: NHEJ-mediated repair of DNA double-strand breaks and BER-mediated repair of DNA single-strand breaks (Koch et al., 2004; Wiederhold et al., 2004). Despite extensive characterization in mammalian systems, functional roles of *pnkp* in zebrafish remain insufficiently defined. To evaluate the influence of *pnkp* deficiency on DNA repair signaling, transcript levels of genes associated with NHEJ- and BER-mediated pathways were analyzed in 5 dpf zebrafish. Within the single-strand break repair network, expression of *ogg1*, *apex1*, *parp1*, and *xrcc1* was elevated, whereas *lig3* expression was reduced (Supplementary Figure S2A). In genes associated with the DNA double-strand break repair pathway, *nhej1* expression increased, while *xrcc6* and *lig4* expression decreased relative to WT zebrafish (Supplementary Figure S2B). These transcriptional alterations indicate that *pnkp* deficiency disrupts both BER and NHEJ DNA repair pathways in zebrafish, supporting a central role of *pnkp* in the maintenance of genomic integrity.

Considering the close relationship between DNA repair processes and DNA damage signaling, the consequences of *PNKP* deficiency on the DNA damage pathway were further examined. Given the technical challenges associated with direct assessment of DNA damage signaling in zebrafish (primarily due to the unavailability of relevant antibodies), experiments were conducted using cultured HEK293T cells following *PNKP* knockdown. Western blot analysis demonstrated an approximately 67% reduction in PNKP expression level in *PNKP* knockdown cells compared with siNC (Supplementary Figure S2C). DNA damage signaling was assessed by quantifying γH2AX, a well-established indicator of DNA double-strand breaks, which exhibited a pronounced increase following *PNKP* depletion, consistent with elevated levels of DNA damage (Supplementary Figure S2D). During DNA damage response, activation of ataxia telangiectasia and Rad3-related kinase (ATR), ataxia telangiectasia-mutated kinase (ATM), and downstream effectors regulates cell cycle progression and promotes apoptotic signaling (Sims et al., 2022). Evaluation of ATR-CHK1 and ATM-CHK2 signaling components revealed increased phosphorylation of ATR, CHK1, and CHK2 (p-ATR, p-CHK1, and p-CHK2), whereas phosphorylated ATM (p-ATM) was reduced in *PNKP*-deficient HEK293T cells (Supplementary Figure S2E). These findings suggest that activation of ATR-dependent signaling represents a major component of the DNA damage response associated with *PNKP* deficiency.

***PNKP* deficiency induces mitochondrial damage**

In addition to nuclear localization, PNKP is present in mitochondria and participates in mtDNA repair (Tahbaz et al., 2012). To determine whether *PNKP* deficiency affects mitochondrial genome integrity, mtDNA damage was evaluated using LR-PCR. Amplification of long mtDNA fragments (8 kb and 8.4 kb) revealed a marked decline in LR-PCR products, indicating increased mtDNA damage under conditions of *PNKP* deficiency (Supplementary Figure S3A). These observations suggest that disruption of PNKP function may adversely affect mitochondrial structure and bioenergetic homeostasis.

Mitochondrial ultrastructure and function were therefore examined through transmission electron microscopy (TEM), transcriptional analysis of mtDNA-encoded genes, and assessment of MMP and oxidative stress. Ultrastructural analysis by TEM demonstrated extensive mitochondrial fragmentation and pronounced disruption of cristae architecture in *PNKP*-deficient HEK293T cells (Supplementary Figure S3B). Consistent with mitochondrial perturbation, transcription of mtDNA-encoded genes *mtATP6* and *mtCytb* was significantly elevated in 5 dpf *pnkp*$^{-/-}$ zebrafish (Supplementary Figure S3C). Functional assessment using JC-1 staining revealed a substantial decrease in MMP in *PNKP*-deficient cells, reflected by a markedly reduced red-to-green fluorescence ratio (Figure 3A). In parallel, intracellular ROS and superoxide dismutase 2 (SOD2) levels, both markers of oxidative stress, were significantly elevated in *PNKP*-deficient HEK293T cells compared to siNC cells (Figure 3B, C). As catalase (CAT), glutathione peroxidase 1 (GPX1), and SOD2 represent major components of cellular antioxidant defense, transcription of corresponding genes was examined in zebrafish. Analysis of 5 dpf *pnkp*$^{-/-}$ zebrafish revealed increased expression of *sod2* and *cat*, while the expression of *gpx1a*, an essential antioxidant enzyme that safeguards cells against oxidative damage, was reduced (Supplementary Figure S3D). These findings demonstrate that *PNKP* deficiency disrupts mitochondrial integrity and promotes oxidative stress, contributing to mitochondrial dysfunction in both zebrafish and HEK293T cells.

Mitochondria constitute highly dynamic organelles that continuously undergo fusion and fission, processes essential for the preservation of mitochondrial function and cellular homeostasis (Kim et al., 2011; Martorell-Riera et al., 2014). Suppression of *PNKP* led to the down-regulation of the OPA1 protein (Figure 3D) and *pnkp* knockout resulted in decreased expression of the *opa1*, *mfn1b*, and *mfn2* genes in zebrafish (Supplementary Figure S3E), consistent with impaired mitochondrial fusion. Alterations in proteins regulating mitochondrial fission were also detected following *PNKP* depletion, characterized by decreased DRP1 and increased DYN2, whereas FIS1 levels remained largely unchanged (Figure 3E). Parallel transcriptional changes were observed in 5 dpf *pnkp*$^{-/-}$ zebrafish, in which the expression levels of *drp1* and *dnm2a* were significantly reduced, while *fis1*, *mffa*, and *dnm2b* transcripts were elevated (Supplementary Figure S3F). Collectively, these observations indicate that *PNKP* activity contributes to the regulation of mitochondrial dynamics and structural integrity in both zebrafish and HEK293T cells.

***pnkp* deficiency triggers mitochondria-mediated apoptosis**

Mitochondrial damage represents a well-established trigger of apoptotic signaling. As *pnkp* deficiency caused microcephaly in zebrafish larvae, apoptosis was evaluated to determine whether abnormal neurodevelopment in *pnkp*$^{-/-}$ larvae was associated with increased cell death. TUNEL analysis performed in 3 dpf larvae showed a significant increase in apoptotic cells within the brains of *pnkp*$^{-/-}$ individuals relative to WT controls (Figure 4A). Because tumor protein p53 functions as a central regulator of apoptosis, p53 expression was quantified at both mRNA and protein levels. Marked elevation of p53 mRNA and protein abundance was detected in 3 dpf *pnkp*$^{-/-}$ larvae (Figure 4B, C), indicating activation of apoptosis-related signaling.

To determine whether apoptosis proceeded through a

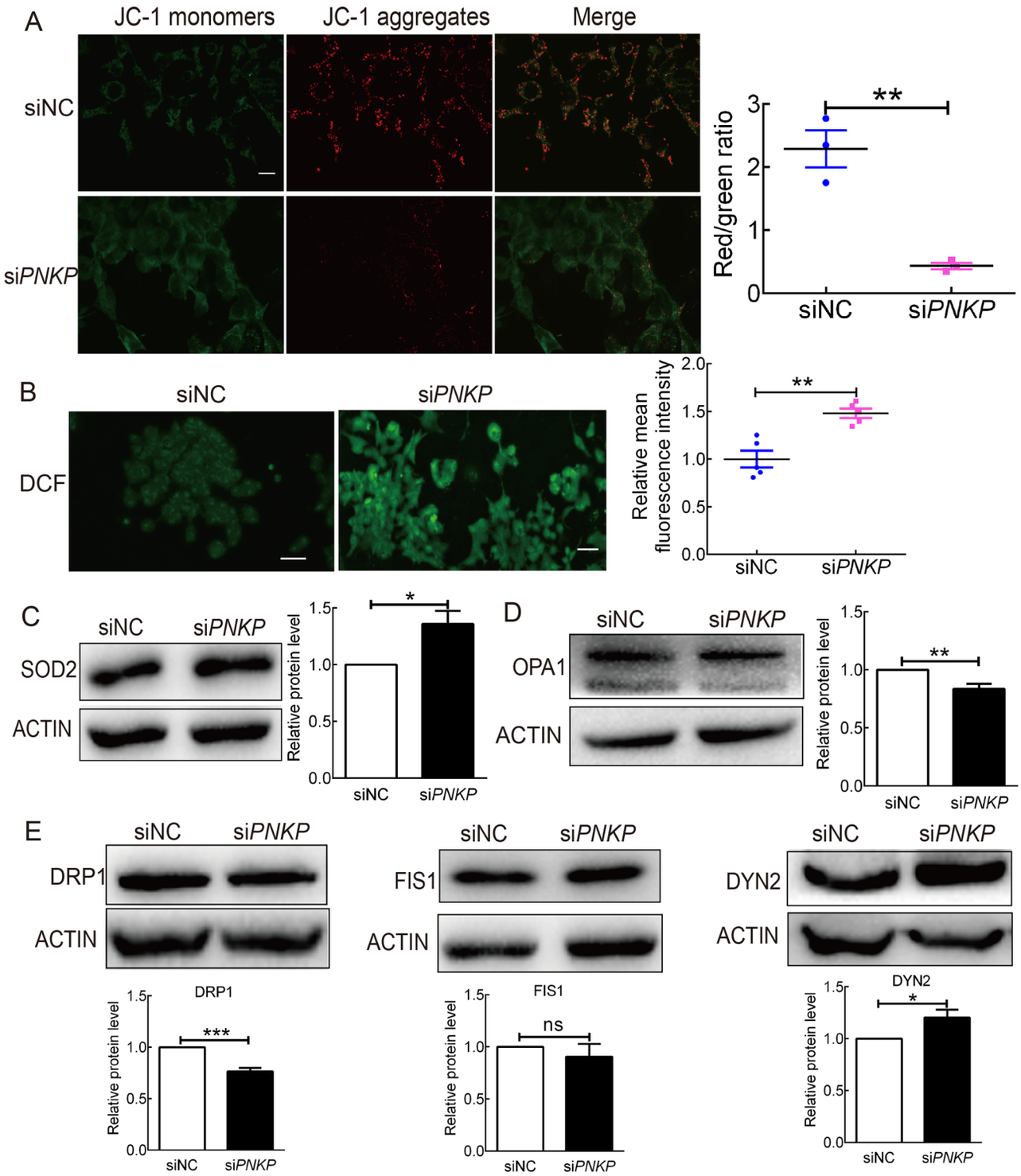

Figure 3 *PNKP* knockdown disrupts mitochondrial function in HEK293T cells

A: Confocal microscopy of MMP measured by JC-1 staining showing a significant decrease in the red/green ratio in si*PNKP* cells compared to siNC (n=3). Scale bar: 20 μm. B: Quantification of intracellular ROS production using DCF fluorescence demonstrating increased mean fluorescence intensity in si*PNKP* cells compared to siNC (n=5). Scale bar: 20 μm. C: Western blot analysis showing significantly elevated SOD2 protein levels in si*PNKP* cells compared to siNC (n=3). D: Western blot analysis showing decreased expression of mitochondrial fusion protein OPA1 in si*PNKP* cells compared to siNC (n=3). E: Western blot analysis of mitochondrial fission proteins showing reduced DRP1 abundance, increased DYN2 abundance, and no significant change in FIS1 in si*PNKP* cells compared to siNC (n≥3). Error bar denotes standard error of the mean (SEM). Significance was determined using unpaired two-tailed Student t-tests. ns: Not significant; *: P<0.05; **: P<0.01; ***: P<0.001; ****: P<0.0001.

mitochondrial pathway, mitochondrial Cyt C release was assessed. Immunofluorescence analysis demonstrated loss of colocalization between Cyt C and the mitochondrial marker protein Mitofilin, indicating translocation of Cyt C from mitochondria to the cytoplasm in *PNKP*-deficient HEK293T cells (Figure 4D, E). Molecular components of the mitochondrial apoptotic cascade were subsequently evaluated. Western blot analysis revealed increased Bax

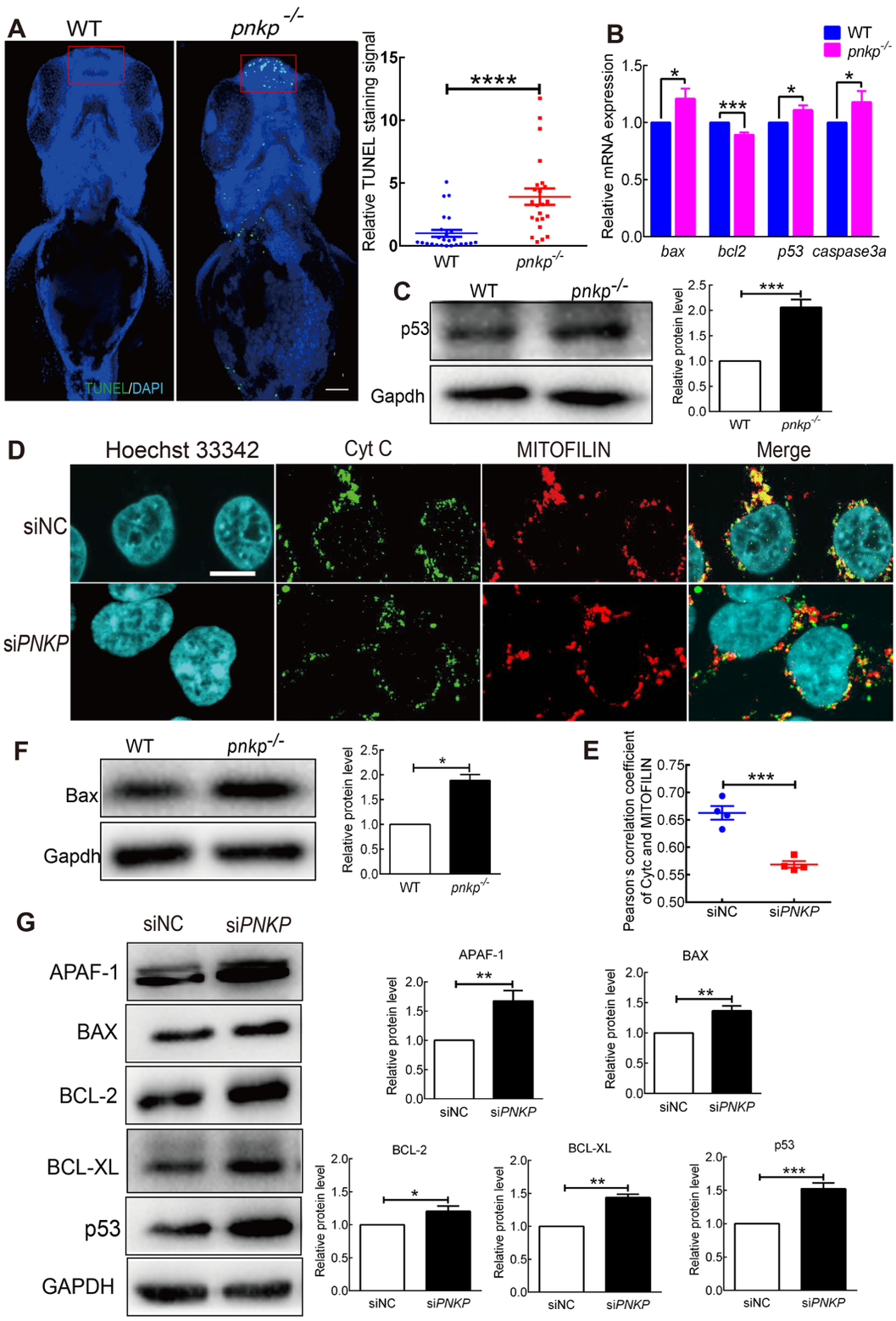

Figure 4 *PNKP* deficiency induces mitochondria-mediated apoptosis

A: Representative image of TUNEL staining showing increased apoptotic cells primarily within brain regions of 3 dpf *pnkp*$^{-/-}$ larvae compared with WT controls (n≥20 per genotype). Red frame indicates regions containing apoptotic signals. Scale bar: 50 μm. B: RT-PCR analysis showing significant up-regulation of key mitochondrial apoptosis-related genes *bax*, *p53*, and *caspase3a* and down-regulation of *bcl2* transcripts in 3 dpf *pnkp*$^{-/-}$ larvae relative to WT controls (n≥3). C: Western blot analysis showing increased p53 protein abundance in 3 dpf *pnkp*$^{-/-}$ larvae compared with WT controls (n=5). D, E: Immunofluorescence analysis of Cyt C and Mitofilin showing reduced colocalization puncta quantified by Pearson correlation coefficients (n=4). Scale bar: 5 μm. F: Western blot analysis showing increased Bax protein abundance in 3 dpf *pnkp*$^{-/-}$ larvae compared with WT controls (n=3). G: Western blot analysis showing increased abundance of mitochondrial apoptosis-related proteins APAF-1, BAX, BCL-2, BCL-XL, and p53 in si*PNKP* HEK293T cells compared with siNC (n≥3). Error bar denotes standard error of the mean (SEM). Significance was determined using unpaired two-tailed Student t-tests. ns: Not significant; *: P<0.05; **: P<0.01; ***: P<0.001; ****: P<0.0001.

protein abundance (Figure 4F), while RT-PCR analysis demonstrated significant up-regulation of *bax* and *caspase3a*, accompanied by reduced expression of *bcl2* (Figure 4B). Consistent with activation of mitochondrial apoptotic signaling, protein expression levels of BAX, BCL-2, BCL-XL, and APAF-1 were markedly increased in *PNKP*-deficient HEK293T cells (Figure 4G). In summary, these results indicate that *pnkp* deficiency triggers apoptotic signaling through both activation of p53-associated pathways and initiation of mitochondria-mediated apoptosis. Increased neuronal apoptosis within developing brain tissue therefore represents a major cellular mechanism contributing to microcephaly observed in *pnkp*$^{-/-}$ zebrafish larvae.

***PNKP* knockdown suppresses autophagy and mitophagy**

Accumulating evidence has established functional links between DNA repair pathways and autophagy regulation (Zhao et al., 2023; Zheng et al., 2019). Given the role of PNKP in DNA repair and cellular responses to DNA damage, potential involvement in autophagic regulation was investigated. Autophagic activity in zebrafish was evaluated through analysis of the autophagosome marker LC3 in *pnkp* knockout larvae. Immunoblot analysis revealed a marked reduction in the Lc3II/Gapdh ratio in *pnkp*$^{-/-}$ zebrafish (Supplementary Figure S4A). After rapamycin treatment, differences in the Lc3II/Gapdh ratio between *pnkp*$^{-/-}$ and WT zebrafish were no longer detectable, supporting reduced basal autophagy in *pnkp*$^{-/-}$ larvae (Supplementary Figure S4B). Autophagic activity was further examined in *PNKP*-silenced cells. A pronounced reduction in the LC3II/LC3I ratio was detected, accompanied by decreased p62 abundance relative to siNC controls (Supplementary Figure S4C). Analysis of additional autophagy-related proteins revealed no detectable change in BECLIN1 expression, whereas ATG5 levels were reduced in *PNKP*-deficient cells (Supplementary Figure S4C). Collectively, these findings suggest that autophagic activity is significantly reduced in both *pnkp*$^{-/-}$ zebrafish and *PNKP*-deficient cells.

Hyperactivation of mammalian target of rapamycin (mTOR), a serine-threonine protein kinase, can function as a central inhibitor of autophagy (Guo et al., 2022). To determine whether altered mTOR signaling contributes to impaired autophagy, protein abundance of mTOR, phosphorylated mTOR (p-mTOR), ribosomal protein S6, and phosphorylated S6 (p-S6) was examined. Significant elevation of p-mTOR and p-S6 levels was detected, whereas total mTOR and S6 levels remained unchanged (Supplementary Figure S4D). Rapamycin treatment markedly increased the LC3II/LC3I ratio in *PNKP*-deficient cells, although p62 levels remained largely unchanged relative to untreated si*PNKP* cells (Supplementary Figure S4E). These findings indicate that activation of mTOR signaling may contribute to suppression of autophagy in *pnkp*$^{-/-}$ zebrafish. Dysregulation of mTOR signaling has been mechanistically associated with seizure through aberrant neuronal excitability (Ravizza et al., 2024). Based on this association, pharmacological inhibition of mTOR signaling with rapamycin was evaluated as a potential strategy to mitigate seizure-related phenotypes caused by *pnkp* deficiency. Acute rapamycin exposure (20 min) reduced hyperactive locomotor behavior in *pnkp*$^{-/-}$ zebrafish during light/dark transitions, repeated light-dark cycles, and startle stimulation conditions (Supplementary Figure S4F–H). Prolonged rapamycin exposure (0.1 μmol/L from 0 hpf to 2 dpf and 0.3 μmol/L from 2 dpf to 5 dpf) similarly alleviated hyperactivity in *pnkp*$^{-/-}$ larvae, whereas locomotor activity in WT larvae remained unaffected under light/dark and light-dark cycling conditions (Supplementary Figure S5A–E). These observations suggest that hyperactivation of mTOR signaling partially contributes to seizure-like behavior associated with *pnkp* deficiency in zebrafish larvae, consistent with previous studies demonstrating that rapamycin alleviates seizure susceptibility in zebrafish (Swaminathan et al., 2018) and reduces epileptic frequency (Parker et al., 2013).

Mitophagy was subsequently evaluated to determine whether *PNKP* deficiency also affects selective mitochondrial turnover. Colocalization analysis between the mitochondrial inner membrane protein COXIV and the autophagosome marker LC3 was performed using immunofluorescence microscopy. Following induction of mitophagy with carbonylcyanide-m-chlorophenylhydrazone (CCCP), colocalization between COXIV and LC3 was markedly reduced in *PNKP*-deficient cells relative to controls (Supplementary Figure S6A). In parallel, reduced abundance of Parkin and PINK1 proteins, key mediators of ubiquitin-related mitophagy, was detected in *PNKP*-deficient cells (Supplementary Figure S6B). These observations were consistent with the reduced mRNA expression levels of *parkin* and *pink1* in *pnkp*$^{-/-}$ zebrafish (Supplementary Figure S3G), suggesting that *PNKP* knockdown reduces mitophagy through the PINK1-Parkin-mediated pathway. Impaired mitophagy was further reflected by accumulation of mitochondrial proteins COXIV and Mitofilin in *PNKP* knockdown cells (Supplementary Figure S6C), consistent with reduced clearance of damaged mitochondria. Taken together, these results indicate that *PNKP* deficiency suppresses mitophagy, resulting in the accumulation of structurally and functionally compromised mitochondria.

Anti-seizure drugs rescue hyperactive behavior in *pnkp*$^{-/-}$ zebrafish larvae

To identify pharmacological interventions capable of mitigating seizure-like phenotypes associated with *PNKP* variants, three clinically used anti-seizure drugs—CBZ, ETX, and LTG—were evaluated. Homozygous *pnkp* mutant zebrafish larvae were used as an *in vivo* screening platform. Larvae were subjected to acute drug exposure (20 min) using concentrations previously reported to be effective in zebrafish behavioral assays (25 μmol/L ETX, 150 μmol/L CBZ, and 100 μmol/L LTG) (Kedra et al., 2020; Milder et al., 2022). Each compound rescued abnormal basal locomotor activity in *pnkp*$^{-/-}$ larvae during light/dark transitions and repeated light-dark cycling paradigms, indicating substantial suppression of seizure- or anxiety-like behavioral phenotypes (Figure 5A, B, D, E, G, H). When larvae were challenged with repeated short dark flashes to provoke startle responses, average velocity of high-velocity movements decreased following ETX, LTG, and CBZ treatment, although locomotor activity did not fully recover to WT levels after acute treatment (Figure 5C, F, I). Among the compounds tested, LTG produced particularly pronounced behavioral improvement, suggesting a strong therapeutic potential for suppression of seizure-like activity associated with *pnkp* deficiency.

To determine whether treatment duration influences drug efficacy, chronic exposure experiments were conducted using ETX, LTG, and CBZ. Similar to the results obtained following acute exposure, prolonged pretreatment (20 h) alleviated

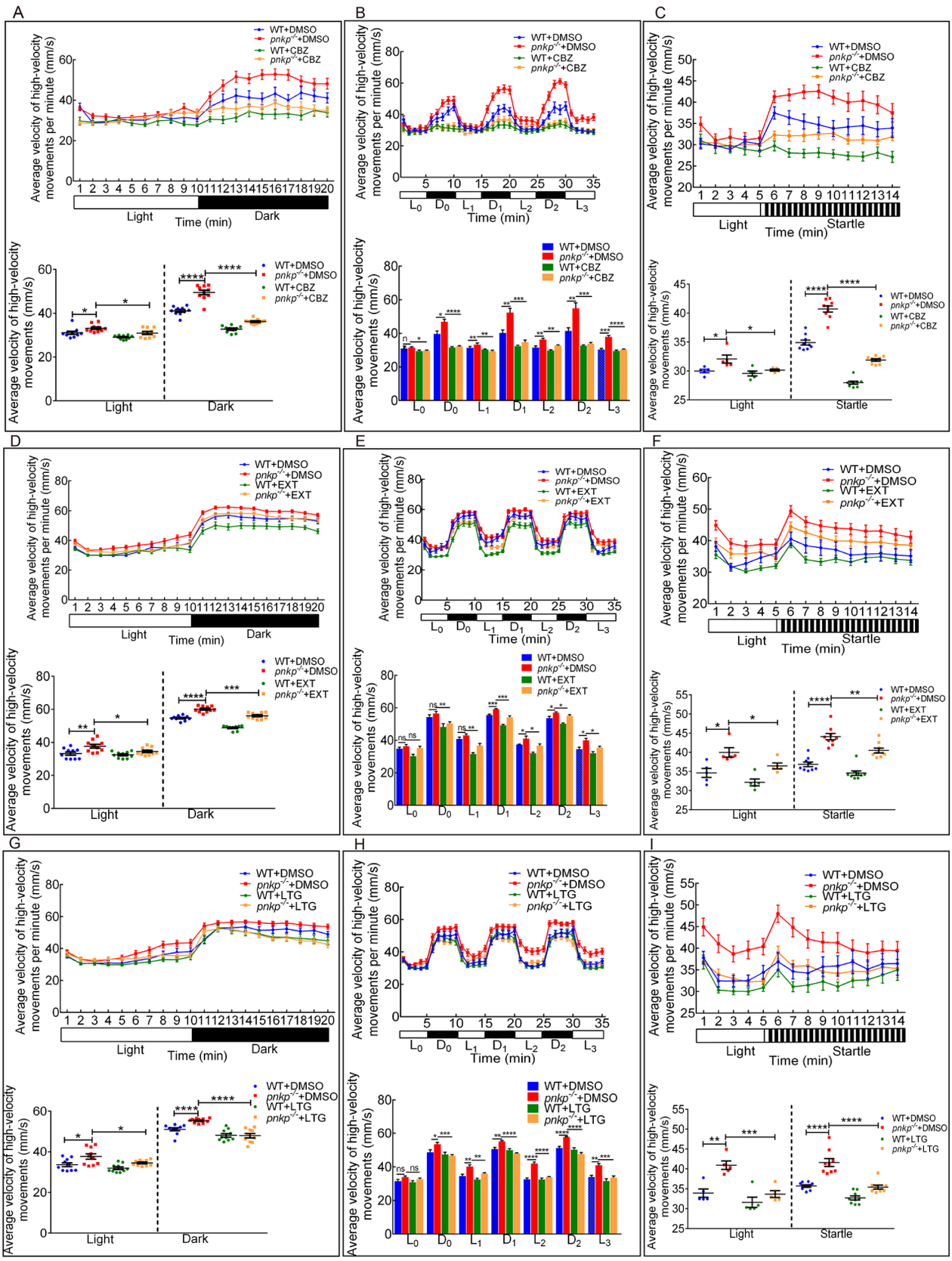

Figure 5 Acute anti-seizure drug treatment effectively alleviates hyperactivity in 5 dpf *pnkp*$^{-/-}$ zebrafish larvae

A–I: Locomotor activity was quantified in WT and *pnkp*$^{-/-}$ zebrafish larvae following acute exposure to DMSO control or anti-seizure drugs ETX (A–C), LTG (D–F), and CBZ (G–I). Behavioral responses were evaluated under light/dark conditions, repeated light-dark cycling, and startle stimulation paradigms (n≥20). Error bar denotes standard error of the mean (SEM). Significance was determined using unpaired two-tailed Student *t*-tests between two groups and one-way analysis of variance (ANOVA) among multiple groups. ns: Not significant; *: P<0.05; **: P<0.01; ***: P<0.001; ****: P<0.0001.

hyperactive locomotor behavior in *pnkp*$^{-/-}$ larvae during light/dark transitions and repeated light-dark cycling (Supplementary Figure S7A–F). Unexpectedly, under startle stimulation, extended CBZ exposure produced a stronger reduction of hyperactivity than acute CBZ treatment in *pnkp*$^{-/-}$ larvae (Supplementary Figure S7G–I). These findings indicate that the therapeutic efficacy of CBZ in this model may be influenced by treatment duration.

pnkp knockout reduces expression of GABA receptor genes in zebrafish larvae

To investigate the transcriptomic consequences of *pnkp* knockout on global gene expression, genome-wide RNA-seq was performed using 5 dpf zebrafish larvae. Differential expression analysis identified 3 051 up-regulated and 3 011 down-regulated DEGs in *pnkp*$^{-/-}$ larvae relative to WT controls (Supplementary Figure S8A). Importantly, KEGG pathway enrichment analysis revealed patterns consistent with earlier experimental observations (Supplementary Figure S8B). GO enrichment analysis further revealed significant enrichment of genes associated with GABA receptor activity and GABA-gated chloride ion channel function (Supplementary Figure S8C). RT-qPCR analysis confirmed these transcriptomic findings and demonstrated reduced expression of multiple GABA receptor genes in *pnkp*$^{-/-}$ larvae (Supplementary Figure S8D), consistent with RNA-seq results. In addition to alterations in GABAergic signaling components, differential expression analysis revealed substantial changes in genes associated with developmental processes, including ubiquitin-dependent protein catabolism, synaptic signaling, and mitochondrial function. These transcriptional alterations suggest accumulation of damaged proteins and disruption of neurodevelopmental pathways, consistent with the developmental delay and seizure-like phenotypes observed in *pnkp*$^{-/-}$ larvae (Supplementary Figure S8C).

To further determine whether GABAergic signaling contributes to seizure-like activity in *pnkp*$^{-/-}$ zebrafish, larvae were administered muscimol, a $GABA_A$ receptor agonist. Pharmacological activation of GABAergic signaling partially rescued the hyperactive locomotor behavior observed in 5 dpf *pnkp*$^{-/-}$ larvae under multiple experimental conditions, including light/dark transitions, repeated light-dark cycling, and repeated short dark-flash stimulation (Supplementary Figure S8E, F, G). These observations indicate that disruption of GABAergic neuronal signaling may contribute to seizure-related behavioral abnormalities associated with *pnkp* deficiency.

DISCUSSION

PNKP contributes to repair of mtDNA, and disruptions in mtDNA maintenance can compromise mitochondrial function, triggering mitochondria-mediated apoptosis and mitophagy (Brandon et al., 2006; Choi et al., 2021). Investigation of *Pnkp* deficiency in mammalian systems has been constrained by embryonic lethality in homozygous knockout mice, hindering analysis of disease pathogenesis *in vivo*. To address this gap, a *pnkp* knockout zebrafish model was established, providing an experimentally tractable vertebrate platform for analysis of pathogenic mechanisms associated with *pnkp* deficiency. Notably, *pnkp*$^{-/-}$ zebrafish larvae exhibited developmental delay, reduced body length, decreased head and brain size, and significant motor behavior abnormalities. Although clinical manifestations such as cerebellar atrophy, intellectual disability, and ataxia vary across affected patients, microcephaly, intractable seizures, and developmental delay remain consistently observed features, supporting emphasis on MCSZ-related phenotypes in this study.

Cellular analyses further demonstrated that *PNKP* deficiency profoundly disrupted mitochondrial quality control pathways. In HEK293T cells, depletion of *PNKP* was associated with reduced MMP, accumulation of ROS, altered mitochondrial dynamics, and activation of mitochondria-mediated apoptotic signaling. Autophagic activity was also reduced through mTOR signaling, whereas impairment of mitophagy was associated with disruption of the PINK1-Parkin pathway. Transcriptomic profiling of *pnkp*$^{-/-}$ zebrafish further revealed altered expression of genes associated with GABAergic signaling. Partial behavioral rescue following treatment with muscimol, a $GABA_A$ receptor agonist, further supported involvement of GABAergic neuronal dysfunction in seizure-like phenotypes observed in *pnkp*$^{-/-}$ zebrafish. In addition, pharmacological screening using *pnkp*$^{-/-}$ larvae identified clinically used anti-seizure agents capable of rescuing seizure- or anxiety-like behavior, with LTG demonstrating particularly promising therapeutic potential.

PNKP has also been detected in mitochondria, where it contributes to maintenance of mitochondrial genome stability through participation in mtDNA repair (Tahbaz et al., 2012). Depletion of PNKP has been shown to destabilize mtDNA and compromise mitochondrial function (Kate et al., 2024). Consistent with these observations, mitochondrial structural abnormalities and functional impairment were detected in both zebrafish and HEK293T cells under conditions of *PNKP* deficiency. Such defects are likely secondary consequences of accumulated mtDNA damage that disrupts mitochondrial homeostasis. Damaged mitochondria are normally removed through mitophagy, a selective autophagic pathway responsible for the elimination of dysfunctional mitochondria (Picca et al., 2023; Zhang et al., 2021). This quality control process is particularly crucial in the central nervous system, where maintenance of mitochondrial integrity limits oxidative stress and supports neuronal energy metabolism, thereby protecting against neurological disorders (Pickrell & Youle, 2015; Zhang et al., 2021). Disruption of PINK1-Parkin signaling detected in the present study indicates impairment of mitophagy under conditions of PNKP deficiency. Consequently, accumulation of damaged mitochondria and impaired mitochondrial turnover may contribute to neurodevelopmental abnormalities associated with *PNKP* deficiency.

Previous studies have reported activation of p53-induced apoptosis in *Pnkp*-deficient mouse models (Shimada et al., 2015), although downstream molecular events remain insufficiently defined. Results from the present study indicated that *pnkp* deficiency induces p53-associated apoptotic signaling in zebrafish larvae, characterized by mitochondrial Cyt C release and elevated BAX abundance, both hallmarks of mitochondria-mediated apoptosis. Increased protein levels of BCL-2 and BCL-XL were also detected, suggesting suppression of autophagic processes, consistent with previous findings demonstrating that *Bcl2* overexpression inhibits autophagy (Xu et al., 2013). The kinases ATM and ATR function as upstream regulators capable of activating p53 and promoting apoptotic signaling (Zuco et al., 2010). Activation of the ATR/CHK1 pathway was observed in *PNKP*-deficient cells, in agreement with earlier reports indicating that

accumulation of DNA lesions following *PNKP* depletion triggers replication checkpoint signaling through the ATR/CHK1 pathway (Sanchez et al., 2017). Collectively, these observations support a model in which *pnkp* deficiency promotes apoptosis through both p53-dependent signaling and mitochondria-mediated pathways. Elevated apoptotic activity may therefore represent a principal driver of microcephaly and neurodevelopmental abnormalities rather than a secondary pleiotropic consequence of cellular stress. Additional studies are required to clarify potential compensatory responses and ancillary signaling pathways that may influence the complexity of this phenotype.

Autophagy represents a highly regulated intracellular process responsible for removal of damaged proteins and organelles and plays critical roles in neuronal survival and epilepsy pathogenesis (Lin et al., 2021). Disruption of autophagic homeostasis, whether excessive or insufficient, can compromise cellular viability. In this study, *PNKP* deficiency impaired autophagic activity and interfered with autophagosome formation and maturation, accompanied by reduced expression of the autophagy-related factor ATG5. Aberrant activation of mTOR has been strongly associated with epileptic disorders (Crino, 2016). Consistent with previous observations (Wang et al., 2021), *pnkp* deficiency was associated with activation of mTOR signaling, a well-established molecular pathway associated with seizure- or anxiety-related behaviors. The present findings further demonstrated that pharmacological inhibition of mTOR signaling using rapamycin partially alleviated hyperactive behavioral phenotypes associated with *pnkp* deficiency, indicating that dysregulated autophagy contributes to seizure-like manifestations in this model.

ETX, LTG, and CBZ are widely used antiepileptic drugs in clinical practice (Shin et al., 2022; Wang et al., 2023). ETX acts primarily through inhibition of T-type Ca^{2+} channels and is commonly applied in the treatment of epilepsy and absence seizures (Miyamoto et al., 2019). LTG is a broad-spectrum antiepileptic drug that primarily suppresses voltage-gated sodium currents and thereby reduces neuronal excitability (Wu et al., 2015). CBZ, a first-generation antiseizure drug, also exerts therapeutic effects through inhibition of voltage-dependent sodium channels (Kanner & Bicchi, 2022). Given that disruption of ion channel activity represents a central mechanism underlying epileptic disorders, pharmacological agents targeting these channels may represent a promising therapeutic strategy. In the present study, treatment with ETX, LTG, and CBZ significantly reduced hyperactive locomotor behavior in *pnkp*$^{-/-}$ zebrafish under both light and dark environments, suggesting that seizure-like neuronal hyperexcitability may contribute to the observed behavioral phenotype. However, high-velocity locomotor bursts in *pnkp*$^{-/-}$ larvae did not fully return to WT levels following either acute exposure or prolonged pretreatment with these agents under startle stimulation conditions. These findings imply that *pnkp*$^{-/-}$ larvae exhibit severe seizure-like activity and may require more specialized pharmacological intervention (Fitton & Goa, 1995). Interestingly, among the compounds tested, LTG produced the most pronounced behavioral improvement, indicating comparatively stronger therapeutic efficacy in this model. Previous studies have shown that LTG can promote autophagic activity in HEK293T cells (Wu et al., 2015), which may partially explain the enhanced therapeutic effect observed in the present study.

KEGG pathway enrichment analysis of RNA-seq data revealed prominent enrichment of genes associated with apoptosis and autophagy, consistent with the experimental observations described above and supporting earlier evidence demonstrating apoptosis in the absence of *Pnkp* (Shimada et al., 2015). GO functional enrichment analysis further identified significant associations between *pnkp* deficiency and biological processes related to oxidative stress response, DNA repair, and mitochondrial function. Enrichment of genes involved in ubiquitin-dependent protein catabolic processes and synaptic signaling also suggested abnormalities in the nervous system and brain development. GABAergic neurons play a crucial role in reducing neuronal excitability and regulating motor behavior (Lahti et al., 2013). Transcriptomic analysis revealed down-regulation of GABA receptor genes in *pnkp*$^{-/-}$ zebrafish, implicating impaired GABAergic signaling in seizure-like behavior. Moreover, pharmacological activation of $GABA_A$ receptors with muscimol partially alleviated hyperactive locomotor behavior, indicating a potential connection between GABAergic neurons and seizure. In contrast, *pnkp*$^{-/-}$ zebrafish did not respond to treatment with the GABA receptor antagonist PTZ (Supplementary Figure S1F), suggesting functional impairment of GABA receptor signaling pathways.

Collectively, our findings indicate that loss of *pnkp* results in accumulation of mtDNA damage and subsequent disruption of mitochondrial integrity. This mitochondrial dysfunction initiates downstream cellular responses, including apoptosis and autophagy, which together contribute to abnormal brain development in zebrafish. Additionally, *pnkp* knockout impairs GABAergic neuronal signaling and promotes seizure-like behavior (Supplementary Figure S8H). Pharmacological analyses further demonstrated that LTG effectively ameliorated hyperactive behavioral phenotypes in the *pnkp*-knockout zebrafish model. Rapamycin and muscimol also exhibited measurable efficacy in reducing seizure-like activity (Supplementary Figure S8E, F, G), suggesting potential therapeutic strategies for neurological manifestations associated with *PNKP* variants. These results establish *pnkp*$^{-/-}$ zebrafish as a valuable vertebrate platform for mechanistic investigation and pharmacological screening, providing an experimental framework for the development of targeted therapeutic interventions for MCSZ associated with *PNKP* deficiency.

DATA AVAILABILITY

The transcriptomic data generated in this study were submitted to the NCBI GEO database (GSE312014), GSA database (accession number CRA031528), and Science Data Bank (doi: 10.57760/sciencedb.j00139.00281.

SUPPLEMENTARY DATA

Supplementary data to this article can be found online.

COMPETING INTERESTS

The authors declare that they have no competing interests.

AUTHORS' CONTRIBUTIONS

X.Q.Z. and Z.K.Z. supervised the study. H.B.J. contributed to methodological development. G.H.W. conceived and performed the experiments, analyzed the data, and wrote the manuscript. L.L.X., W.M.J., Z.X.L., Y.X.S., X.Q.Z., and Z.K.Z. revised the manuscript. All authors read and approved the final version of the manuscript.

ACKNOWLEDGMENTS

We thank the Research Core Facilities for Life Science (HUST).

REFERENCES

Akbari M, Nilsen HL, Montaldo NP. 2022. Dynamic features of human mitochondrial DNA maintenance and transcription. *Frontiers in Cell and Developmental Biology*, **10**: 984245.

Baechler BL, Bloemberg D, Quadrilatero J. 2019. Mitophagy regulates mitochondrial network signaling, oxidative stress, and apoptosis during myoblast differentiation. *Autophagy*, **15**(9): 1606–1619.

Baronio D, Chen YC, Decker AR, et al. 2022. Vesicular monoamine transporter 2 (SLC18A2) regulates monoamine turnover and brain development in zebrafish. *Acta Physiologica*, **234**(1): e13725.

Bernstein NK, Williams RS, Rakovszky ML, et al. 2005. The molecular architecture of the mammalian DNA repair enzyme, polynucleotide kinase. *Molecular Cell*, **17**(5): 657–670.

Brandon M, Baldi P, Wallace DC. 2006. Mitochondrial mutations in cancer. *Oncogene*, **25**(34): 4647–4662.

Chen YP, Wu JH, Liang G, et al. 2020. CHK2-FOXK axis promotes transcriptional control of autophagy programs. *Science Advances*, **6**(1): eaax5819.

Choi GE, Lee HJ, Chae CW, et al. 2021. BNIP3L/NIX-mediated mitophagy protects against glucocorticoid-induced synapse defects. *Nature Communications*, **12**(1): 487.

Crino PB. 2016. The mTOR signalling cascade: paving new roads to cure neurological disease. *Nature Reviews Neurology*, **12**(7): 379–392.

Damas J, Samuels DC, Carneiro J, et al. 2014. Mitochondrial DNA rearrangements in health and disease--a comprehensive study. *Human Mutation*, **35**(1): 1–14.

Dan XL, Babbar M, Moore A, et al. 2020. DNA damage invokes mitophagy through a pathway involving Spata18. *Nucleic Acids Research*, **48**(12): 6611–6623.

Dhir A. 2012. Pentylenetetrazol (PTZ) kindling model of epilepsy. *Current Protocols in Neuroscience*, **58**(1).

Fitton A, Goa KL. 1995. Lamotrigine: an update of its pharmacology and therapeutic use in epilepsy. *Drugs*, **50**(4): 691–713.

Fontana GA, Gahlon HL. 2020. Mechanisms of replication and repair in mitochondrial DNA deletion formation. *Nucleic Acids Research*, **48**(20): 11244–11258.

Gahl RF, Dwivedi P, Tjandra N. 2016. Bcl-2 proteins bid and bax form a network to permeabilize the mitochondria at the onset of apoptosis. *Cell Death & Disease*, **7**(10): e2424.

Guo HR, Ouyang YJ, Yin H, et al. 2022. Induction of autophagy via the ROS-dependent AMPK-mTOR pathway protects copper-induced spermatogenesis disorder. *Redox Biology*, **49**: 102227.

Huang DW, Sherman BT, Lempicki RA. 2009. Systematic and integrative analysis of large gene lists using DAVID bioinformatics resources. *Nature Protocols*, **4**(1): 44–57.

Kalasova I, Hailstone R, Bublitz J, et al. 2020. Pathological mutations in PNKP trigger defects in DNA single-strand break repair but not DNA double-strand break repair. *Nucleic Acids Research*, **48**(12): 6672–6684.

Kanner AM, Bicchi MM. 2022. Antiseizure medications for adults with epilepsy: a review. *JAMA*, **327**(13): 1269–1281.

Kate WD, Fanta M, Weinfeld M. 2024. Loss of the DNA repair protein, polynucleotide kinase/phosphatase, activates the type 1 interferon response independent of ionizing radiation. *Nucleic Acids Research*, **52**(16): 9630–9653.

Kedra M, Banasiak K, Kisielewska K, et al. 2020. TrkB hyperactivity contributes to brain dysconnectivity, epileptogenesis, and anxiety in zebrafish model of Tuberous Sclerosis Complex. *Proceedings of the National Academy of Sciences of the United States of America*, **117**(4): 2170–2179.

Kim J, Kundu M, Viollet B, et al. 2011. AMPK and mTOR regulate autophagy through direct phosphorylation of Ulk1. *Nature Cell Biology*, **13**(2): 132–141.

Koch CA, Agyei R, Galicia S, et al. 2004. Xrcc4 physically links DNA end processing by polynucleotide kinase to DNA ligation by DNA ligase IV. *The EMBO Journal*, **23**(19): 3874–3885.

Lahti L, Achim K, Partanen J. 2013. Molecular regulation of GABAergic neuron differentiation and diversity in the developing midbrain. *Acta Physiologica*, **207**(4): 616–627.

Lin QS, Li S, Jiang N, et al. 2021. Inhibiting NLRP3 inflammasome attenuates apoptosis in contrast-induced acute kidney injury through the upregulation of HIF1A and BNIP3-mediated mitophagy. *Autophagy*, **17**(10): 2975–2990.

Liu J, Fang HB, Chi ZF, et al. 2015. XPD localizes in mitochondria and protects the mitochondrial genome from oxidative DNA damage. *Nucleic Acids Research*, **43**(11): 5476–5488.

Liu PF, Qian LM, Sung JS, et al. 2008. Removal of oxidative DNA damage via FEN1-dependent long-patch base excision repair in human cell mitochondria. *Molecular and Cellular Biology*, **28**(16): 4975–4987.

Martorell-Riera A, Segarra-Mondejar M, Muñoz JP, et al. 2014. Mfn2 downregulation in excitotoxicity causes mitochondrial dysfunction and delayed neuronal death. *The EMBO Journal*, **33**(20): 2388–2407.

Milder PC, Zybura AS, Cummins TR, et al. 2022. Neural activity correlates with behavior effects of anti-seizure drugs efficacy using the zebrafish pentylenetetrazol seizure model. *Frontiers in Pharmacology*, **13**: 836573.

Miyamoto H, Tatsukawa T, Shimohata A, et al. 2019. Impaired cortico-striatal excitatory transmission triggers epilepsy. *Nature Communications*, **10**(1): 1917.

Parker WE, Orlova KA, Parker WH, et al. 2013. Rapamycin prevents seizures after depletion of STRADA in a rare neurodevelopmental disorder. *Science Translational Medicine*, **5**(182): 182ra53.

Picca A, Faitg J, Auwerx J, et al. 2023. Mitophagy in human health, ageing and disease. *Nature Metabolism*, **5**(12): 2047–2061.

Pickrell AM, Youle RJ. 2015. The roles of PINK1, Parkin, and mitochondrial fidelity in Parkinson's disease. *Neuron*, **85**(2): 257–273.

Ravizza T, Scheper M, Di Sapia R, et al. 2024. mTOR and neuroinflammation in epilepsy: implications for disease progression and treatment. *Nature Reviews Neuroscience*, **25**(5): 334–350.

Reynolds JJ, Walker AK, Gilmore EC, et al. 2012. Impact of PNKP mutations associated with microcephaly, seizures and developmental delay on enzyme activity and DNA strand break repair. *Nucleic Acids Research*, **40**(14): 6608–6619.

Riley BE, Lougheed JC, Callaway K, et al. 2013. Structure and function of Parkin E3 ubiquitin ligase reveals aspects of RING and HECT ligases. *Nature Communications*, **4**(1): 1982.

Sanchez A, Gadaleta MC, Limbo O, et al. 2017. Lingering single-strand breaks trigger Rad51-independent homology-directed repair of collapsed replication forks in the polynucleotide kinase/phosphatase mutant of fission yeast. *PLoS Genetics*, **13**(9): e1007013.

Shen J, Gilmore EC, Marshall CA, et al. 2010. Mutations in *PNKP* cause microcephaly, seizures and defects in DNA repair. *Nature Genetics*, **42**(3): 245–249.

Shimada M, Dumitrache LC, Russell HR, et al. 2015. Polynucleotide kinase-phosphatase enables neurogenesis via multiple DNA repair pathways to maintain genome stability. *The EMBO Journal*, **34**(19): 2465–2480.

Shin JN, Lee KB, Butterworth W, et al. 2022. Zebrafish EEG predicts the efficacy of antiepileptic drugs. *Frontiers in Pharmacology*, **13**: 1055424.

Shin W, Alpaugh W, Hallihan LJ, et al. 2021. PNKP is required for maintaining the integrity of progenitor cell populations in adult mice. *Life Science Alliance*, **4**(9): e202000790.

Sims JR, Faça VM, Pereira C, et al. 2022. Phosphoproteomics of ATR signaling in mouse testes. *eLife*, **11**: e68648.

Swaminathan A, Hassan-Abdi R, Renault S, et al. 2018. Non-canonical mTOR-independent role of DEPDC5 in regulating GABAergic network development. *Current Biology*, **28**(12): 1924–1937. e5.

Tahbaz N, Subedi S, Weinfeld M. 2012. Role of polynucleotide kinase/phosphatase in mitochondrial DNA repair. *Nucleic Acids Research*, **40**(8): 3484–3495.

Wang J, Huang PY, Yu QW, et al. 2023. Epilepsy and long-term risk of arrhythmias. *European Heart Journal*, **44**(35): 3374–3382.

Wang TT, Zhou MS, Zhang Q, et al. 2021. *ubtor* mutation causes motor hyperactivity by activating mTOR signaling in zebrafish. *Neuroscience Bulletin*, **37**(12): 1658–1670.

Wiederhold L, Leppard JB, Kedar P, et al. 2004. AP endonuclease-independent DNA base excision repair in human cells. *Molecular Cell*, **15**(2): 209–220.

Winter MJ, Redfern WS, Hayfield AJ, et al. 2008. Validation of a larval zebrafish locomotor assay for assessing the seizure liability of early-stage development drugs. *Journal of Pharmacological and Toxicological Methods*, **57**: 176–187.

Withers SE, Rowlands CF, Tapia VS, et al. 2023. Characterization of a mutant *samhd1* zebrafish model implicates dysregulation of cholesterol biosynthesis in Aicardi-Goutières syndrome. *Frontiers in Immunology*, **14**: 1100967.

Wu H, Lu MH, Wang W, et al. 2015. Lamotrigine reduces β-site AβPP-cleaving enzyme 1 protein levels through induction of autophagy. *Journal of Alzheimer's Disease*, **46**(4): 863–876.

Wu MQ, Liu XY, Chi XS, et al. 2018. Mitophagy in refractory temporal lobe epilepsy patients with hippocampal sclerosis. *Cellular and Molecular Neurobiology*, **38**(2): 479–486.

Xu HD, Wu D, Gu JH, et al. 2013. The pro-survival role of autophagy depends on Bcl-2 under nutrition stress conditions. *PLoS One*, **8**(5): e63232.

Zhang LJ, Dai L, Li DY. 2021. Mitophagy in neurological disorders. *Journal of Neuroinflammation*, **18**(1): 297.

Zhao F, Zhu JF, Zhang MJ, et al. 2023. OGG1 aggravates renal ischemia-reperfusion injury by repressing PINK1-mediated mitophagy. *Cell Proliferation*, **56**(8): e13418.

Zheng J, Croteau DL, Bohr VA, et al. 2019. Diminished OPA1 expression and impaired mitochondrial morphology and homeostasis in Aprataxin-deficient cells. *Nucleic Acids Research*, **47**(8): 4086–4110.

Zuco V, Benedetti V, Zunino F. 2010. ATM- and ATR-mediated response to DNA damage induced by a novel camptothecin, ST1968. *Cancer Letters*, **292**(2): 186–196.